Polymorphism and Alloys in the Bis(ethylenedithio)tetrathiafulvalene/$M(CN)_4^{2-}$ Radical Cation Salts. Structural and Physical Properties of α,δ-$(ET)_4[Ni(CN)_4]_x[Pt(CN)_4]_{1-x}(H_2O)_n$

M. Fettouhi, L. Ouahab,* and D. Grandjean

Laboratoire de Chimie du solide et Inorganique Moléculaire, URA 1495 CNRS, Université Rennes I, 35042 Rennes Cédex, France

L. Ducasse*

Laboratoire de Physico-Chimie Théorique, URA 503 CNRS Université Bordeaux I, 33405 Talence Cédex, France

J. Amiell, R. Canet, and P. Delhaès*

Centre de Recherche Paul Pascal CNRS, avenue Albert Schweitzer, 33600 Pessac, France

Received May 25, 1994. Revised Manuscript Received December 6, 1994[⊗]

The synthesis and structural and physical properties of some radical cation salts based on bis(ethylenedithio)tetrathiafulvalene (BEDT-TTF) and tetracyanometallates $M(CN)_4^{2-}$ (M = Pt(II) and Ni(II)) are reported. The salts $(ET)_4[Ni(CN)_4]_x[Pt(CN)_4]_{1-x}(H_2O)_n$ ($x = 0-1$; $n = 0-4$) have been isolated with different principal packing modes, in particular the α and δ types. In both cases the structures consist of alternating layers of organic cations and inorganic anions, and two different kinds of packing, namely, α_1 and α_2, have been observed in the case of the α type structure. The organic sublattice in the α_1 salts is built of two independent chains, while only one type of dimerized chain is observed in the α_2 modification. The δ phase is originated from an independent and strongly dimerized one-dimensional stack. All materials are conductors at ambient temperature and exhibit a semiconducting behavior upon cooling. For the α_1 phase the spin susceptibility and the ESR line widths decrease with temperature, giving rise to two anomalies respectively at about 200 and 20 K. The α_2 type shows a classical Currie–Weiss low-T dependence of the spin susceptibility with a Weiss temperature $\theta = -25$ K, characteristic of weak antiferromagnetic interactions. In the case of the δ type a strong decrease of the spin susceptibility at about 180 K reminiscent of a Peierls-type transition is observed. The band calculations (EHT model) agree with the observed ambient temperature conducting behavior for both α and δ phases. The nesting of the Fermi surface for the latter type might be related to the occurrence of a structural phase transition. In the absence of nesting for the α_1 type, an alternative mechanism based on the alternation of electronic densities on the different intermolecular bonds (bond order wave) is proposed to explain the observed electronic localization at low temperature. Finally a general description of the polymorphism encountered with their related structural organization is proposed.

Introduction

Most of the known organic radical cation salts are based on TTF (tetrathiafulvalene) type molecules and monovalent and diamagnetic anions.[1] Over several years, we have developed a program aimed to search for new molecular materials based on inorganic anions which differ from the commonly used ones by their charge, size, shape, and electronic properties.[2] The main goals are (i) the modification of the electronic or magnetic dimensionality which plays a great role in the low-temperature physical properties, and (ii) the preparation of conducting and/or magnetic materials by mixing organic and inorganic sublattices in order to reveal unusual physical properties.

Many charge transfer complexes based on BEDT-TTF and tetracyanometallates have been reported by several groups,[2,3] with three kinds of packing modes, namely, the α, β, and δ modes.[1,4] The κ phase is absent in the ET series but it can be found in the salts κ-$(MDT)_4M(CN)_4(solv)_x$ based on the unsymmetrical donor MDT-TTF (methylenedithiotetrathiafulvalene).[5] Recently superconductivity has been detected in the hydrated salts β-$(ET)_4M(CN)_4(H_2O)$, M = Pt(II) and Pd(II),[6] while the anhydrous ones exhibit only a semiconducting behav-

* To whom correspondence should be addressed.

[⊗] Abstract published in *Advance ACS Abstracts,* February 1, 1995.

(1) Williams, J. M.; Ferraro, J. R.; Thorn, R. J.; Carlson, K. D.; Geiser, U.; Wang, H. H.; Kini, A. M.; Whangbo, M. H. *Organic Superconductors*; Prentice-Hall: New York, 1992; Inorganic and Organometallic Chemistry Series.

(2) Ouahab, L.; Padiou, J.; Grandjean, D.; Garrigou-Lagrange, C.; Delhaes, P.; Bencharif, M. *J. Chem. Commun.* **1989**, *1038*. (b) Garrigou-Lagrange, C.; Ouahab, L.; Grandjean, D.; Delhaes, P. *Synth. Met.* **1990**, *35*, 9. (c) Fettouhi, M.; Ouahab, L.; Grandjean, D.; Amiell, J.; Canet, R.; Delhaes, P. *Synth. Met.* **1993**, *56*, 1893.

0897-4756/95/2807-0461$09.00/0

ior.[2,3] Therefore this result attracted considerable attention on electrocrystallization in aqueous media. In this context our goal is to explore all the packing modes potentially possible for ET/$M(CN)_4^{2-}$ (M = Pt(II) and Ni(II)) as well as to study the partial alloying effect on the structural and physical properties of these materials. This kind of substitution has been reported for other systems for both the organic component and the anionic part.[7] In the present paper we describe the preparation and the characterization of new alloys of chemical formula α,δ-$(ET)_4[Ni(CN)_4]_x[Pt(CN)_4]_{1-x}(H_2O)_n$, $x = 0-1$; $n = 0-4$. The X-ray crystal structures and electrical and ESR measurements are presented on the basis of the usual structural classification,[1] and finally a comparative theoretical study within the semiempirical extended Hückel theory (EHT) with other similar compounds has been conducted. Then a general discussion about the presented rich polymorphism is proposed.

Experimental Section

Starting Compounds. The preparation of the $(R_4N)_2M(CN)_4$ salts has been conducted according to the literature[8] or by direct precipitation in aqueous media as follows. These compounds were prepared by treating a concentrated aqueous solution (25 mL, 0.75 M) of $K_2M(CN)_4$ with a 2-fold excess of the corresponding tetraalkylammonium bromide (10 mL, 2.36 M). The microcrystalline compound was collected by filtration and washed several times with ether. The air dried product can be recrystallized from acetonitrile. The salts of the dianions $[M(CN)_4]^{2-}$ have the following formulas: $[(n\text{-}C_4H_9)_4N]_2Pt(CN)_4$ and $[(C_2H_5)_4N]_2Ni(CN)_4(H_2O)_{1.5}$. Anal. Calcd for $[(n\text{-}C_4H_9)_4N]_2Pt(CN)_4$: C, 55.14; H, 9.26; N, 10.71; Pt, 24.68. Found: C, 54.82; H, 9.35; N, 10.76; Pt, 24.70. Anal. Calcd for $[(C_2H_5)_4N]_2Ni(CN)_4(H_2O)_{1.5}$: C, 53.35; H, 9.63; N, 18.67; Ni, 13.04. Found: C, 54.15; H, 10.11; N, 18.65; Ni, 12.45.

Electrocrystallization. The title compounds were obtained on a platinum wire electrode by anodic oxidation of the organic donor BEDT-TTF (5×10^{-3} M) under constant current ($J = 1.3\ \mu A/cm^2$) in the presence of tetraalkylammonium salts of the dianions (10^{-2} M) as supporting electrolyte. The time of crystal growth at room temperature was between 1 and 2 weeks. The different phases may be obtained depending on the type of solvent. When the electrocrystallization is carried out in solvents such as dichloromethane, dimethylformamide, or 1,1,2 trichloroethane, the main product is the β-phase previously reported,[2,3] while a mixture (1/1) of tetrahydrofuran and 1,1,2-trichloroethane gives crystals of the α_1 phase as the major product: α_1-$(ET)_4[Pt(CN)_4]$ (**1**) and α_1-$(ET)_4[Ni(CN)_4]$ (**2**) are thus obtained. Standard electrocrystallization using mixtures of organic solvents and water, for instance dichloromethane or trichloroethane as a heterogeneous mixture and dimethylformamide (3%), leads to large black plates and thin needles of the δ phase. Despite the observed morphological difference between these crystals, ESR results showed that only one kinetic phase is obtained and the X-ray structure analysis and the thermogravimetric investigations revealed the presence of water molecules. Such phase (δ) is present in a poor ratio in other batches obtained using nondried solvents. The stoichiometries obtained by X-ray analysis are respectively δ-$(ET)_4Pt(CN)_4$ (**3**) and δ-$(ET)_4Ni(CN)_4(H_2O)_4$ (**4**). The Ni/Pt alloys have been obtained as nice brown crystals when electrocrystallization is performed with a 1/1 mixture of $[(n\text{-}C_4H_9)_4N]_2Pt(CN)_4$ and $[(C_2H_5)_4N]_2Ni(CN)_4$ in dimethylformamide for α_1-$(ET)_4[Ni(CN)_4]_{0.55}[Pt(CN)_4]_{0.45}$ (**5**) and a mixture of 1,1,2-trichloroethane and water for δ-$(ET)_4[Ni(CN)_4]_{0.48}[Pt(CN)_4]_{0.52}(H_2O)_4$ (**6**). The use of $K_2M(CN)_4(H_2O)_x$, M = Pt, Ni, with a 1/1 proportion, in dried 1,1,2-trichloroethane gives a major product, α_2-$(ET)_4[Ni(CN)_4]_{0.14}[Pt(CN)_4]_{0.86}(H_2O)_4$ (**7**).

X-ray Diffraction. The X-ray data collections were performed on an Enraf-Nonius CAD4 diffractometer equipped with a graphite-monochromatized Mo Kα ($\lambda = 0.710\ 73$ Å) radiation. The unit-cell parameters were determined and refined from setting angles of 25 accurately centered reflections. Data were collected with the $\theta-2\theta$ scan method and intensities were corrected for Lorentz and polarization effects. The structures at room temperature were solved by direct methods and successive Fourier difference synthesis. An empirical absorption correction was applied using the DIFABS procedure.[9] The refinements (on F) were performed by the full-matrix least-squares method [H atoms, both found by Fourier synthesis and placed at computed positions (C−H 1 Å, $B = 5$ Å^2), were not refined]. Distribution of the Pt and Ni in the heavy atom positions was determined by placing a Pt and a Ni atom in each metal site and constraining their positional and thermal parameters to remain identical for the atoms in each site. The same procedure has been used for the anionic C atoms and the O atoms of the water molecules in the case of compounds **3** and **6**. Population parameters were constrained to total 1 for each site. The scattering factors were taken from the *International Tables for X-ray Crystallography* (1974). All the calculations were performed on a MicroVAX 3100 using the SDP and Molen programs.[10]

Electrical Conductivity and Electron Spin Resonance Measurements. The dc electrical conductivity measurements over the range 4−300 K have been performed on single crystals by the standard four-probe method. The electrical contacts on crystals were made directly by gold wires using silver paint. The ESR experiments on single crystals have been done with an X-band Varian spectrometer equipped with an Oxford Instruments variable-temperature accessory (4−300 K). The crystals were mounted with silicone grease on a quartz rod. The field was calibrated using the diphenylpicrylhydrazyl free radical (DPPH, $g = 2.0037$) as a reference. For each phase several crystals were employed to check the reproducibility of the presented results, i.e., linewidths S in gauss and g-factor values.

Band Structure Calculations. The transfer integrals, band structure, and Fermi surface of the title compounds have been obtained following the procedure used previously[11] within the semiempirical extended Hückel theory (EHT).[12]

Results

Room-Temperature Crystal Structures. The crystal data of all compounds are presented in Table 1a, where the usual α, β, δ nomenclature is used.[1] The atomic coordinates of **5**−**7** representing the α_1, δ, and

(3) (a) Shibaeva, R. P.; Lobkovskaya, R. M.; Korotkov, V. B.; Kushch, N. D.; Yagubskii, E. B.; Makova, M. K. *Synth. Met.* **1988**, *27*, A457. (b) Lobkovskaya, R. M.; Kushch, N. D.; Shibaeva, R. P.; Yagubskii, E. B.; Simonov, M. A. *Kristallografiya* **1989**, *34*, 698. (c) Tanaka, M.; Takuchi, H.; Sano, M.; Enoki, T.; Suzuki, K.; Imaeda, K. *Bull. Chem. Soc. Jpn.* **1989**, *62*, 1432. (d) Gartner, S.; Heinen, H.; Keller, H. J.; Niebl, R.; Nuber, B.; Schweitzer, D. *Naturforsch.* **1990**, *45*, 763. (e) Tanaka, M.; Takeuchi, H.; Kawamato, A.; Tanaka, J.; Enoki, T.; Suzuki, K.; Imaeda, K.; Inokuchi, H. In Saito, G., Kagoshima, Eds.; *The Physics and Chemistry of Organic Superconductors*; Springer: Berlin, 1990; p 298. (f) Kawamato, A.; Tanaka, M.; Tanaka, J. *Bull. Chem. Soc. Jpn.* **1991**, *64*, 3160.

(4) The structure of the α-$(ET)_4Pt(CN)_4$ and the physical characterization of the δ-$(ET)_4Pt(CN)_4$ have been reported by Gartner et al.[3d] We present here a more accurate X-ray structure of the first one for comparison with the alloys structural and physical characteristics.

(5) (a) Mousdis, G. A.; Ducasse, L.; Fettouhi, M.; Ouahab, L.; Dupart, E.; Garrigou-Lagrange, C.; Amiell, J.; Canet, R.; Delhaes, P. *Synth. Met.* **1992**, *48*, 219. (b) Ducasse, L.; Mousdis, G. A.; Fettouhi, M.; Ouahab, L.; Amiell, J.; Delhaes, P. *Synth. Met.* **1993**, *56*, 1995.

(6) Mori, H.; Hirabayashi, I.; Tanaka, S.; Mori, T.; Muruyama, Y.; Inokushi, H. *Solid State Commun.* **1991**, *80*, 411.

(7) (a) Coulon, C.; Delhaes, P.; Amiell, J.; Manceau, J. P.; Fabre, J. M.; Giral, L. *J. Phys.* **1982**, *43*, 1721. (b) Laversanne, R. Thesis of Bordeaux University, 1985.

(8) Mason, R. W.; Gray, H. B. *J. Am. Chem. Soc.* **1968**, *21*, 5721.

(9) Walker, N.; Stuart, D. *Acta Crystallogr.* **1983**, *A39*, 158.

(10) (a) Frenz, B. A. and Associates Inc., 1985. SDP Structure Determination Package, College Station, TX, and Enraf-Nonius, Delft, The Netherlands. (b) Crystal Structure Analysis, Molecular Enraf-Nonius (MolEN)1990, Delft Instruments X-Ray Diffraction, B. V. Rontgenweg 1 2624 BD Delft, The Netherlands.

(11) Ducasse, L.; Abderrabba, A.; Hoarau, J.; Pesquer, M.; Gallois, B.; Gaultier, J. *J. Phys. C: Solid State Phys.* **1986**, *19*, 3805.

(12) Hoffmann, R. *J. Chem. Phys.* **1963**, *39*, 1397.

Table 1

(a) Crystal Data of $(ET)_4[Ni(CN)_4]_x[Pt(CN)_4]_{1-x}(H_2O)_y$

	1	**2**	**3**	**4**	**5**	**6**	**7**
phase	α_1	α_1	δ	δ	α_1	δ	α_2
x	0	1	1	0	0.55	0.48	0.14
y	0	0	4	0	0	4	4
a (Å)	11.149(4)	11.123(5)	17.403(4)	17.466(8)	11.199(17)	17.413(4)	9.019(6)
b	33.459(4)	33.313(6)	6.767(9)	6.771(7)	33.490(7)	6.742(1)	11.051(6)
c	16.504(3)	16.506(3)	15.030(3)	15.084(4)	16.571(4)	15.026(3)	32.317(12)
β (deg)	91.52(2)	91.41(5)	109.26(2)	108.92(2)	91.28(5)	109.17(2)	92.12(5)
SG	*C*2/*c*	*C*2/*c*	*P*2/*c*	*P*2/*c*	*C*2/*c*	*P*2/*c*	$P2_1/n$
dc (g/cm^3)	1.984	1.846	1.727	1.808	1.882	1.836	1.956
Z	4	4	1	1	4	1	2
M (g)	1837.9	1701.5	1737.56	1837.91	1769.72	1844.52	1890.89
V (Å^3)	6154	6114	1670	1687	6213	1666	3209
R	0.029		0.052	0.054	0.037	0.042	0.043
Rw	0.038		0.064	0.082	0.046	0.053	0.052
uni data	5385		2795	2898	5255	3483	5722
uni obs data with $I \geq n\sigma(I)$	3358 (n = 6)		1320 (n = 3)	2148 (n = 3)	3145 (n = 3)	1469 (n = 3)	3554 (n = 3)
GOF	1.07		1.53	2.06	1.12	1.22	1.31

(b) Atomic Coordinates and Equivalent Isotropic Thermal Parameters for α_1-$(ET)_4[Ni(CN)_4]_{0.55}[Pt(CN)_4]_{0.45}$ (**5**)

atom	x	y	z	B (Å^2)	atom	x	y	z	B (Å^2)
Pt	0	0.22876(2)	0.25	3.22(1)	C3	0.0020(4)	0.0663(2)	−0.1307(3)	2.4(1)
Ni	0	0.22876	0.25	3.22	C4	0.0536(5)	0.1406(1)	−0.1486(3)	2.5(1)
S1	0.1209(1)	0.09414(4)	−0.16616(9)	2.78(3)	C5	−0.0571(5)	0.1402(1)	−0.1175(3)	2.5(1)
S2	−0.1180(1)	0.09328(4)	−0.09569(9)	2.95(3)	C6	−0.0401(6)	0.2204(2)	−0.0786(5)	6.5(2)
S3	−0.1467(1)	0.18096(4)	−0.0944(1)	3.73(3)	C7	0.0845(7)	0.2123(2)	−0.0848(5)	7.7(2)
S4	0.1376(1)	0.18355(4)	−0.16577(9)	3.42(3)	C8	0.0037(5)	0.0253(2)	−0.1291(3)	2.7(1)
S5	0.1215(1)	−0.00292(4)	−0.16450(9)	3.17(3)	C9	0.0594(5)	−0.0490(1)	−0.1394(3)	2.6(1)
S6	−0.1151(1)	−0.00207(4)	−0.0911(1)	3.33(3)	C10	−0.0498(5)	−0.0485(1)	−0.1056(3)	2.6(1)
S7	0.1482(1)	−0.08992(4)	−0.1640(1)	3.49(3)	C11	0.0685(6)	−0.1302(2)	−0.1197(4)	4.8(2)
S8	−0.1349(1)	−0.08904(4)	−0.0745(1)	3.80(3)	C12	−0.0623(6)	−0.1291(2)	−0.1251(5)	5.1(2)
S9	0.6221(1)	0.04815(4)	0.5359(1)	3.49(3)	C13	0.5002(5)	0.0204(2)	0.5005(3)	2.9(1)
S10	0.3790(1)	0.04861(4)	0.4644(1)	3.46(3)	C14	0.5599(5)	0.0949(1)	0.5127(3)	2.7(1)
S11	0.3586(1)	0.13651(4)	0.45626(9)	3.30(3)	C15	0.4477(5)	0.0951(1)	0.4807(3)	2.7(1)
S12	0.6522(1)	0.13529(4)	0.5382(1)	3.41(3)	C16	0.4343(5)	0.1750(1)	0.5142(3)	2.8(1)
S13	0.6221(1)	0.04200(4)	0.7858(1)	3.58(3)	C17	0.5670(5)	0.1777(2)	0.5000(3)	3.1(1)
S14	0.6477(1)	0.12925(4)	0.79029(9)	3.25(3)	C18	0.5	0.0136(2)	0.75	2.8(2)
S15	0.3800(1)	−0.05451(4)	0.7109(1)	3.42(3)	C19	0.5562(5)	0.0882(1)	0.7659(3)	2.7(1)
S16	0.3539(1)	−0.14210(4)	0.70656(9)	3.32(3)	C20	0.5664(5)	0.1694(2)	0.7427(3)	2.9(1)
N1	−0.1991(6)	0.2302(2)	0.1176(4)	6.6(2)	C21	0.5	−0.0266(2)	0.75	2.9(2)
N2	−0.1933(5)	0.2271(2)	0.3784(4)	6.2(1)	C22	0.4450(4)	−0.1014(1)	0.7329(3)	2.7(1)
C1	−0.1250(6)	0.2297(2)	0.1661(4)	4.6(1)	C23	0.4330(5)	−0.1827(2)	0.7559(3)	3.2(1)
C2	−0.1219(6)	0.2285(2)	0.3316(4)	4.4(1)					

(c) Atomic Coordinates and Equivalent Isotropic Thermal Parameters for δ-$(ET)_4[Ni(CN)_4]_{0.48}[Pt(CN)_4]_{0.52}(H_2O)_4$ (**6**)

atom	x	y	z	B (Å^2)	atom	x	y	z	B (Å^2)
Pt	0	0	0	2.81(3)	S6	0.6462(1)	0.2050(3)	0.1117(2)	2.73(5)
Ni	0	0	0	2.81	S7	0.8162(1)	0.2759(4)	0.1275(2)	3.88(6)
C1	−0.0045(6)	0.033(2)	0.1174(6)	8.0(3)	S8	0.7704(1)	0.7709(3)	0.1556(2)	4.20(6)
O1	−0.0045	0.033	0.1174	8.0	C3	0.4988(4)	0.322(1)	0.1200(5)	2.1(2)
C2	−0.0458(5)	0.275(2)	−0.0373(6)	7.6(3)	C4	0.5751(4)	0.375(1)	0.1217(5)	2.1(2)
O2	−0.0458	0.275	−0.0373	7.6	C5	0.7231(4)	0.376(1)	0.1243(5)	2.0(2)
N1	0.0029(8)	0.071(2)	0.199(1)	4.6(4)	C6	0.7061(4)	0.568(1)	0.1360(6)	2.5(2)
N2	−0.056(1)	0.427(3)	−0.057(1)	6.6(5)	C7	0.8801(5)	0.483(2)	0.151(1)	7.5(4)
S1	0.2598(1)	0.4181(3)	0.1221(2)	3.01(5)	C8	0.8650(5)	0.651(2)	0.1959(9)	7.1(4)
S2	0.3139(1)	−0.0807(4)	0.1200(2)	5.32(7)	C9	0.3518(4)	0.319(1)	0.1214(5)	2.0(2)
S3	0.4264(1)	0.4926(3)	0.1227(2)	2.67(5)	C10	0.3719(4)	0.128(1)	0.1192(6)	2.5(2)
S4	0.4688(1)	0.0752(3)	0.1144(2)	2.92(5)	C11	0.2010(5)	0.203(2)	0.113(1)	8.4(4)
S5	0.6076(1)	0.6193(3)	0.1356(2)	2.88(5)	C12	0.2198(5)	0.021(2)	0.1013(9)	7.6(3)

(d) Atomic Coordinates and Equivalent Isotropic Thermal Parameters for α_2-$(ET)_4[Ni(CN)_4]_{0.14}[Pt(CN)_4]_{0.86}(H_2O)_4$ (**7**)

atom	x	y	z	B (Å^2)	atom	x	y	z	B (Å^2)
Pt	0	0	0	3.071(8)	C2	−0.1404(9)	0.1336(8)	−0.0115(2)	4.2(2)
Ni	0	0	0	3.071	C3	0.062(1)	−0.0535(8)	0.1150(2)	4.6(2)
S1	0.1011(2)	0.1486(2)	0.16533(6)	4.04(4)	C4	0.0523(9)	0.0804(8)	0.1155(2)	4.1(2)
S2	0.9340(2)	−0.1334(2)	0.14607(5)	3.70(4)	C5	0.9892(8)	0.0640(7)	0.1979(2)	2.9(1)
S3	0.9565(2)	0.1341(2)	0.24507(5)	3.59(4)	C6	0.9293(8)	−0.0439(6)	0.1902(2)	2.5(1)
S4	0.8205(2)	−0.1057(2)	0.22952(5)	3.17(4)	C7	0.8521(7)	0.0148(6)	0.2643(2)	2.7(1)
S5	0.8223(2)	0.1400(2)	0.33570(5)	3.25(4)	C8	0.7962(7)	0.0156(7)	0.3024(2)	2.9(1)
S6	0.6902(2)	−0.1019(2)	0.32217(5)	3.04(4)	C9	0.7353(7)	0.0726(6)	0.3781(2)	2.7(1)
S7	0.7412(2)	0.1597(2)	0.23426(5)	3.76(4)	C10	0.6774(7)	−0.0371(6)	0.3719(2)	2.7(1)
S8	0.5901(2)	−0.1297(2)	0.40746(6)	3.91(4)	C11	0.699(2)	0.048(1)	0.4598(3)	9.6(3)
S9	0.6336(2)	0.1570(2)	0.11788(6)	3.82(4)	C12	0.601(1)	−0.0418(9)	0.4536(3)	6.5(2)
S10	0.4717(2)	−0.1284(2)	0.10128(6)	4.12(4)	C13	0.560(2)	−0.031(1)	0.0656(3)	10.4(3)
S11	0.5273(2)	0.1275(2)	0.20246(5)	3.15(4)	C14	0.613(2)	0.070(1)	0.0736(3)	14.2(4)
S12	0.3960(2)	−0.1093(2)	0.18822(5)	3.09(4)	C15	0.5420(7)	0.0666(7)	0.1530(2)	2.8(1)
S13	0.4002(2)	0.1263(2)	0.29555(5)	3.06(4)	C16	0.4799(7)	−0.0443(6)	0.1466(2)	2.5(1)
S14	0.2564(2)	−0.1035(2)	0.27763(5)	3.36(4)	C17	0.4244(7)	0.0115(6)	0.2216(2)	2.6(1)
S15	0.3010(2)	0.1451(2)	0.38129(6)	3.49(4)	C18	0.3670(7)	0.0124(6)	0.2605(2)	2.6(1)
S16	0.1249(2)	−0.1318(2)	0.35861(6)	4.48(4)	C19	0.3029(7)	0.0623(7)	0.3355(2)	2.6(1)
O	0.0170(9)	0.170(1)	0.5120(3)	9.8(3)	C20	0.2351(8)	−0.0454(6)	0.3270(2)	3.0(1)
N1	0.2506(9)	0.1897(8)	0.0182(2)	6.1(2)	C21	0.160(1)	−0.0630(9)	0.4079(3)	6.1(2)
N2	−0.2190(9)	0.2119(8)	−0.0181(2)	5.9(2)	C22	0.1644(9)	0.0667(8)	0.4102(2)	4.6(2)
C1	0.1595(9)	0.1209(8)	0.0117(2)	4.3(2)					

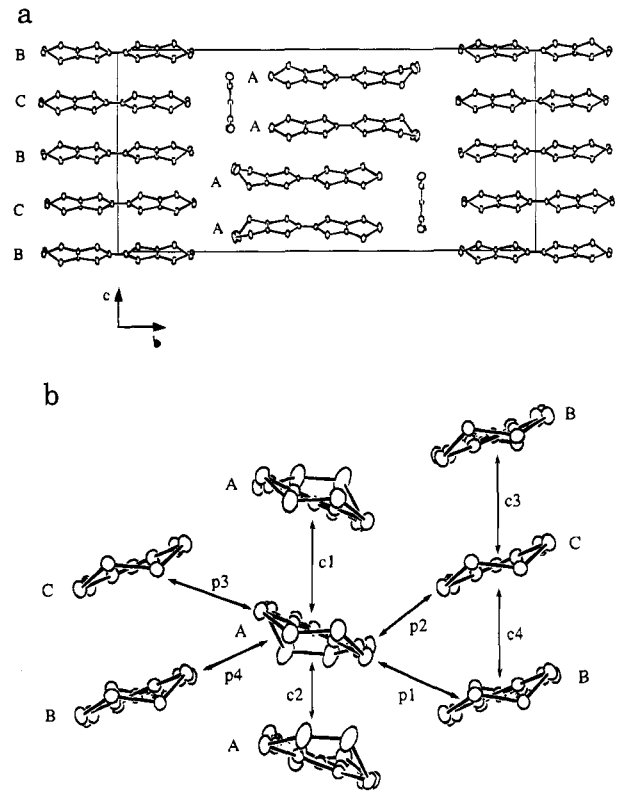

Figure 1. Crystal structure of **5**: (a) stacking mode along the chains; (b) projection along the main molecular axis showing the labeling of the transfer integrals.

α_2 structural types respectively are given in Table 1b–d. The additional atomic coordinates, thermal parameters, bond angles, and bond distances are given as supplementary material (see paragraph at end of table).

All the crystal structures are built of alternating layers of the organic donors and the inorganic anions as known in such type of materials. However, the main difference lies first in the packing mode of each chain and second in the way these chains pack to generate the organic layer.[1]

In the α organic sublattice the unit cell contains two layers and the normals to the molecular planes, located on two adjacent stacks, are inclined with opposite direction and the dihedral angles between the molecules are in the range of 50°. Two structural modifications have been obtained.

In the α_1-$(ET)_4[Ni(CN)_4]_x[Pt(CN)_4]_{1-x}$ ($x = 0, 0.55, 1$)[4] three independent molecules (A, B, C) generate two molecular stacks. They are located on a general position, inversion center, and 2-fold axis, respectively (Figure 1). The first chain is based exclusively on the A molecule [AAAA...] arranged in a dimerized manner where the interdimer packing mode is characterized by an important displacement in the main molecular axis direction. The second chain adopts the [BCBC...] packing scheme with no such displacement. The two interstack dihedral angles (A–B ≈47°; A–C ≈49°) are particularly lower when compared to the values observed for the superconducting α- and θ-$(ET)_2X$ salts.[1] Besides many interstack contacts are observed and characterized by short S–S distances lower than the van der Waals sum radii (Table 2a). An identical organic structural scheme is encountered in the recent reported salts based on polyoxometallate anions.[13] Despite the significant difference between the two anion units concerning their charge,[14] size, and symmetry, the ET molecules do build a quasi-identical 2D framework. Unlike α_1, the α_2 structural type in $(ET)_4[Ni(CN)_4]_{0.14}[Pt(CN)_4]_{0.86}(H_2O)_4$ is generated by only two independent molecules both located on a general position and giving rise to one independent dimerized chain, [ABAB...] (Figure 2). In this case the dimer components show a slight shift along the minor molecular axis and dimers are displaced in the main molecular axis direction as observed in [AAAA...] chain of the α_1 phase.

The δ organic sublattice, observed in the salts $(ET)_4[Ni(CN)_4]_x[Pt(CN)_4]_{1-x}(H_2O)_y$, shows particular molecular stacks parallel to the *c* direction, where twisted ET dimers are rotated with respect to each other about

Table 2

(a) Interactions between ET Molecules[a]

compound	molecule	t_{ij}	atoms	S–S
1(5)	A(I)–A(II)	*c*1		>3.65
	A(I)–A(III)	*c*2		>3.65
	A(I)–B(I+a)	*p*1	S1–S12	3.530(3.551)
			S4–S12	3.504(3.521)
			S7–S10	3.558(3.586)
			S7–S11	3.405(3.424)
	A(I)–C(I+*a*)	*p*2	S1–S14	3.540(3.545)
			S7–S15	3.554(3.559)
			S7–S16	3.625(3.631)
	A(I)–C(I)	*p*3	S2–S14	3.395(3.417)
			S3–S14	3.414(3.428)
	A(I)–B(I)	*p*4	S3–S11	3.642(>3.65)
			S8–S9	3.571(3.582)
			S8–S12	3.424(3.428)

(b) Interactions between ET Molecules[b]

	molecules	t_{ij}	atoms	S–S
3(**4**)(**6**)[c]	(I)–(I±*b*)	*b*	S1–S2	3.533(3.521)(3.514)
			S3–S2	3.482(3.490)(3.474)
			S8–S6	3.574(3.594)(3.568)
			S8–S7	3.567(3.564)(3.568)
	(I)–(II+*a*)	*a*1		>3.65
	(I)–(II+*a*+*b*)	*ab*1		>3.65
	(I)–(III+*a*±*b*)	*ab*2		>3.65
	(I)–(III+*a*)	a_2		>3.65
7[b]	A(I)–B(I)	a_1		>3.65
	A(I)–B(I+a)	a_2		>3.65
	A(I)–B(II+b)	b_1	S1–S14	3.515
			S1–S16	3.568
			S7–S10	3.601
	A(I)–B(II)	b_2	S2–S13	3.552
			S2–S15	3.555
			S6–S9	3.622
			S8–S9	3.547
	A(I)–A(II)	b_3	S2–S5	3.472
			S2–S7	3.529
	B(I)–B(II–a+b)	b_4	S9–S16	3.404
			S11–S16	3.554
			S15–S10	3.568

[a] Short S–S contacts (<3.65 Å, in angstroms) for **1** and **5** (values in parentheses). The interaction labeling correspond to that of Mori et al.[28] on α-$(ET)_2[MHg(SCN)_4]$ (see Figure 1b). A(I): *x*, *y*, *z*. A(II): -*x*, -*y*, -*z* − ½. A(III): -*x*, *y*, -*z* − ½. B(I): [-*x*, *y*, ½ − *z*, and *x* − 1, -*y*, *z* − ½]. C(I): [*x* − 1, *y*, *z* − 1, and -*x*, *y*, ½ − *z*]. [b] Short S–S contacts (<3.65 Å, in angstroms) for **3** (**4** and **6** in parentheses) and **7**. The interaction labeling depicted in Figures 2b and 3c for **7** and **6** respectively corresponds to that of Mori eta l.[28] on α-$ET_2[MHg(SCN)_4]$. [c] (I): *x*, *y*, *z*. (II) -*x*, -*y*, -*z*. (III) -*x*, *y*, ½ − *z*. [d] A(I): *x*, *y*, *z*. A(II) ³/₂ − *x*, *y* − ½, ½ − *z*. B(II) ³/₂ − *x*, *y* − ½, ½ − *z*.

(13) Gomez-Garcia, C. J.; Ouahab, L.; Gimenez-Saiz, C.; Triki, S.; Coronado, E.; Delhaes, P. *Angew. Chem., Int. Ed. Engl.* **1994**, *33*, 223.
(14) Lemagueres, P.; Ouahab, L.; Gomez-Garcia, C. J.; Delhaes, P., to be published.

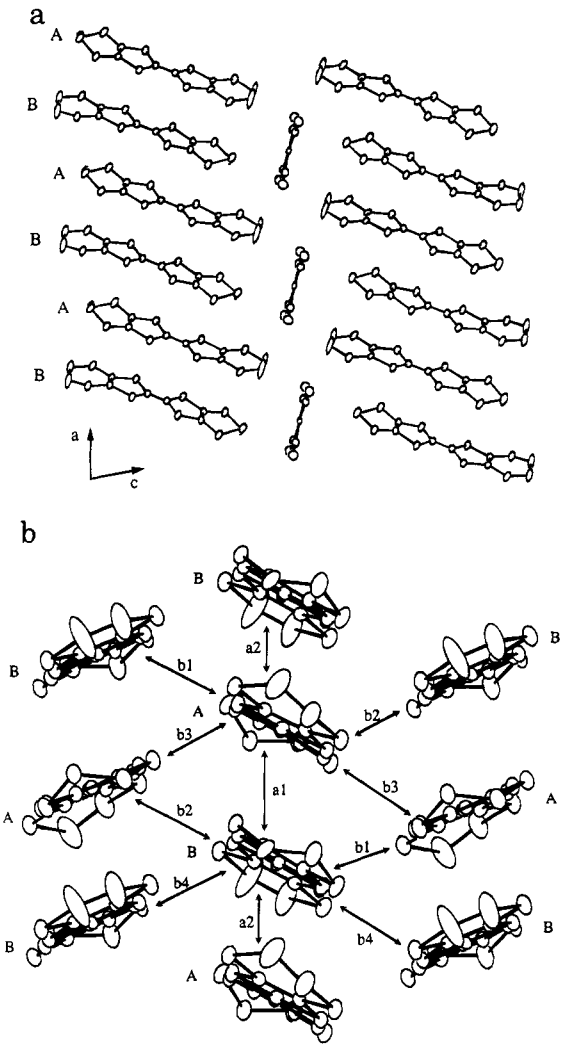

Figure 2. Crystal structure of **7**: (a) stacking mode along the chains; (b) projection along the main molecular axis showing the labeling of the transfer integrals.

the stacking axis by about 30° (Figure 3). The anionic unit is located on the inversion center (2a) of the *P2/c* space group with an occupancy factor of 0.5 on the (0,0,0) and (0,0,1/2) positions. The second position is occupied by a four H_2O molecules motif; the same molecular arrangement has been reported for the salt $(ET)_4Pt(CN)_4(C_2H_3Cl_3)$.[15] The ET chains are strongly dimerized and present weak interdimer contacts associated to unfavorable molecular orientations as observed in the $\alpha'(ET)_2X$ series (X = $AuBr_2^-$, $CuCl_2^-$, and $Ag(CN)_2^-$).[16]

In the alloys α_1-, α_2-, and δ-$(ET)_4[Ni(CN)_4]_{1-x}[Pt(CN)_4]_x(H_2O)_y$, the Ni and Pt atoms have been found to occupy statistically the special positions of the corresponding space group (Table 1a). The examination of these structures reveals no major difference with respect to the Pt and Ni salts. Nevertheless a slight increase in the interstack S−S distances is noticed between the α_1-Pt and α_1-$[Ni_{0.48}Pt_{0.52}]$ salts (Table 2a,b).

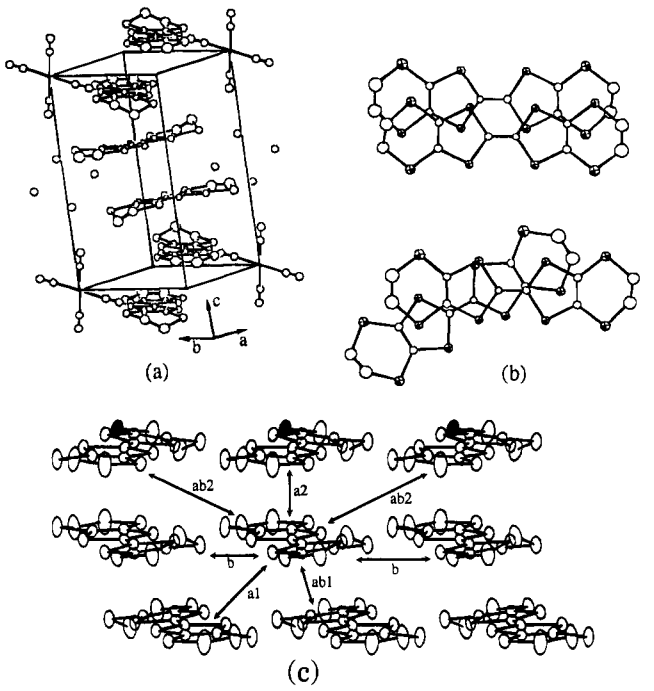

Figure 3. Crystal structure of **6**: (a) unit cell; (b) stacking modes of the ET molecules along the *c* direction; (c) projection along the main molecular axis showing the labeling of the transfer integrals.

Table 3. Comparison of the Averaged Intramolecular Distances (Å) for Various Observed Charges on the ET Molecules

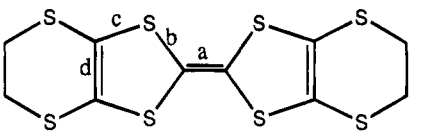

		a	*b*	*c*	*d*	ϱ_{ref}	ϱ_{cal}[a]	ϱ_{tot}	ref
		1.319(10)	1.757(10)	1.753(10)	1.331(10)	0			34
		1.360(10)	1.732(9)	1.744(9)	1.340(10)	+1/2			28
		1.388(10)	1.720(11)	1.737(10)	1.345(15)	+1			35
		1.436(7)	1.669(6)	1.710(6)	1.369(7)	+2			3a
1	A	1.354(7)	1.737(5)	1.742(5)	1.348(7)		0.52	2.2	
	B	1.366(6)	1.733(5)	1.746(5)	1.351(7)		0.68		
	C	1.356(9)	1.743(4)	1.754(4)	1.335(7)		0.49		
5	A	1.381(8)	1.735(5)	1.747(5)	1.357(8)		0.82	2.4	
	B	1.365(7)	1.745(6)	1.754(3)	1.351(8)		0.57		
	C	1.340(10)	1.755(4)	1.753(5)	1.351(7)		0.23		
3	A	1.360(10)	1.736(8)	1.744(8)	1.33(1)		0.59	2.4	
4	A	1.338(9)	1.748(7)	1.748(7)	1.34(1)		0.26	1.0	
6	A	1.355(9)	1.733(7)	1.743(7)	1.33(1)		0.56	2.2	
7	A	1.345(9)	1.751(7)	1.759(7)	1.33(1)		0.31	2.3	
	B	1.372(9)	1.719(7)	1.732(7)	1.36(1)		0.86		

[a] Using the relation $a/b = 0.751 + 0.0548\varrho$, from ref 16.

To estimate the electronic charge transfer in these salts, we have used the relation established by Umland et al.[17] between the bond length ratio and the degree of ionicity in the ET salts. It appears that for all compounds the calculated values are closed to the stoichiometric charge ($\varrho = 2$), except for compound **4** for which the erroneous calculated value is due to low accuracy of the structure determination (Table 3) coming from unresolved disorder on the anionic cyanide positions.

Physical Properties. *Electrical Properties.* The room-temperature (RT) values are summarized in Table 4. They are distributed over about 4 orders of magni-

(15) Lobkovskaya, R. M.; Shibaeva, R. P.; Kushch, N. D.; Yagubskii, E. V. *Sov. Phys. Crystallog.* **1990**, *35*, 1.

(16) (a) Beno, M. A.; Firestone, M. A.; Leung, P. c. W.; Sowa, L. M.; Wang, H. H.; Williams, J. M.; Whangbo, M. H. *Solid State Commun.* **1986**, *57*, 735. (b) Geiser, U.; Wang, H. H.; Hammond, C. E.; Firestone, M. A.; Beno, M. A.; Carlson, K. D.; Nunez, L.; Williams, J. M. *Acta Crystallogr.* **1987**, *C43*, 656. (c) Kurmoo, M.; Talham, D. R.; Pritchard, K. L.; Day, P.; Stringer, A. M.; Howard, J. A. K. *Synth. Met.* **1988**, *27*, A177.

(17) Umland, T. C.; Allie, S.; Huhlmann, T.; Coppens, P. *J. Phys. Chem.* **1988**, *92*, 6456.

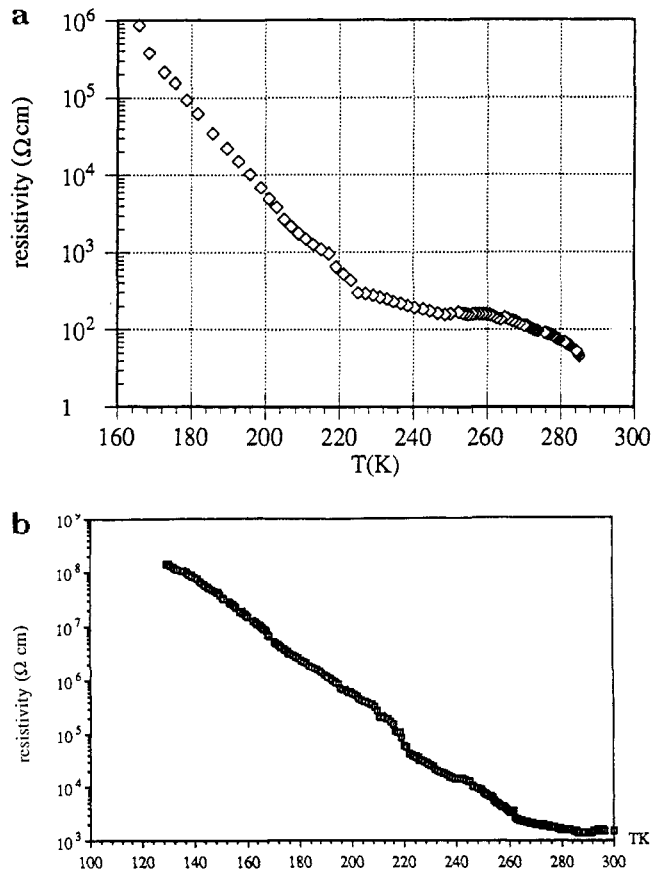

Figure 4. Temperature dependences of the resistivity for (a) α_1-$(ET)_4[Ni(CN)_4]_{0.55}[Pt(CN)_4]_{0.45}$ (**5**) and (b) α_2-$(ET)_4[Ni(CN)_4]_{0.14}[Pt(CN)_4]_{0.86}(H_2O)_4$ (**7**).

tude and for all structural types the temperature dependences show low-temperature activated regimes. In the case of **1** ($\sigma_{RT} \approx 5$ S cm^{-1}) two semiconducting regimes are observed between 280 and 245 K ($E_a = 425$ meV) and below 245 K ($E_a = 915$ meV). For the alloy **5** ($\sigma_{RT} \approx 0.2$ S cm^{-1}) two regimes have been also detected with similar activation energies (Figure 4a). The α_2 phase presents a lower absolute room-temperature conductivity ($\sigma_{RT} \approx 10^{-3}$ S cm^{-1}), but behavior similar to the α_1 one is noticed when lowering temperature (Figure 4b). Finally for the δ phase (compounds **4** and **6**) the temperature dependences depicted in Figure 5a,b exhibit also a progressive electronic localization below 180 K.

ESR Measurements. We have examined the g value and line-width (S) anisotropies at room temperature (see Table 4) which present an almost collinear main axis. For the line positions, the principal values are phase dependent because they are sensitive to the local organization. However, the tensor trace is almost constant because this is rather a molecular characteristic.[1] Concerning the line widths, differences are observed because the ESR relaxation times are a function of the electronic dimensionality: it is generally admitted that the RT absolute value is increasing with the effective dimensionality.[18] It appears therefore that the δ phase shows a narrower ESR line than the β and the α-phases as expected from the less pronounced 2D character indicated by the crystal structure studies. For the temperature dependences, we have selected several

(18) Delhaes, P.; Amiell, J.; Flandrois, S.; Ducasse, L.; Fritsch, A.; Hiliti, B.; Mayer, C. W.; Zambounis, J. S.; Papavassiliou, G. C. *J. Phys.* **1990**, *51*, 1179.

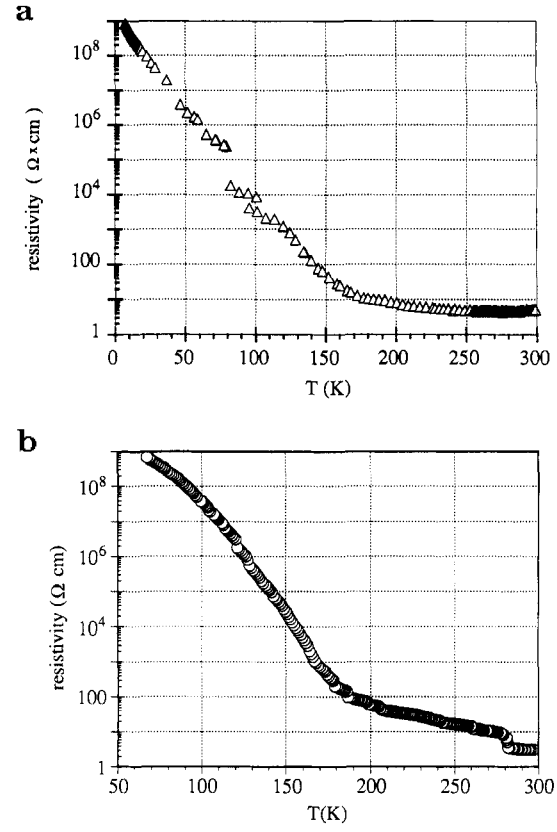

Figure 5. Temperature dependences of the resistivity for (a) δ-$(ET)_4[Pt(CN)_4]$ (**3**) and (b) δ-$(ET)_4[Ni(CN)_4]_{0.48}[Pt(CN)_4]_{0.52}(H_2O)_4$ (**6**).

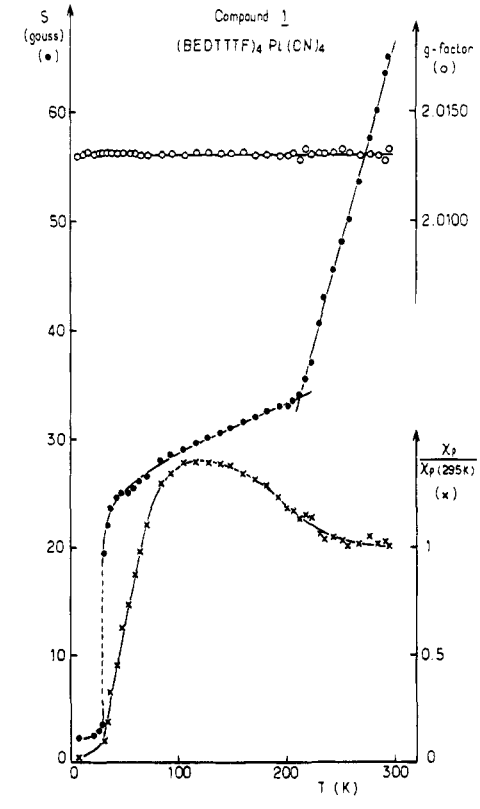

Figure 6. Temperature dependences of the g factor, ESR line width, and spin susceptibility for α_1-$(ET)_4[Pt(CN)_4]$ (**1**).

results which are presented on Figures 6–8 for the α_1, α_2, and δ phases, respectively. All these results are presented for a selected crystal orientation inside the resonance cavity corresponding to g_{max} and S_{max} (see Table 4). The α_1 phase presents a rather surprising line

Table 4. Room-Temperature ESR Characteristics and Dc Electrical Conductivity Values for the Different Phases

	β phase[2]		δ-phase			α_1-phase		α_2-phase
	Pt	Ni	Pt **3**	Ni **4**	Pt/Ni **6**	Pt **1**	Pt/Ni **5**	Pt/Ni **7**
ESR								
g factors								
g_{min}	2.0029	2.0024	2.0023	2.0023	2.0025	2.0027	2.0026	2.0056
g_{int}		2.0067	2.0068	2.0066	2.0068		2.0055	2.0066
g_{max}	2.0127	2.0130	2.0105	2.0110	2.0110	2.0130	2.0112	2.0114
line widths								
S_{min}	26	26	17	18	19	38	36	30
S_{int}		32	23	23	24	–	40	34
S_{max}	38	40	28	28	28	63	62	36
conductivity								
σ_{dc} (S cm^{-1})	10	2		10^{-1}	$3\ 10^{-1}$	5	2×10^{-1}	$\approx 10^{-3}$

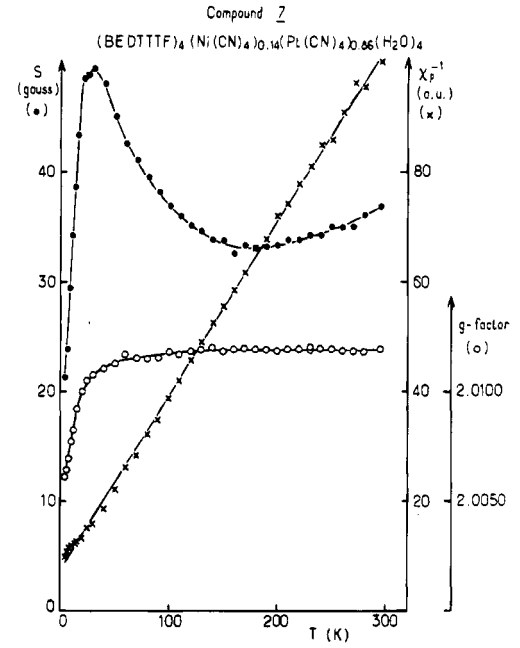

Figure 7. Temperature dependences of the *g* factor, ESR line width, and spin susceptibility for α_2-(ET)$_4$[Ni(CN)$_4$]$_{0.14}$[Pt(CN)$_4$]$_{0.86}$(H$_2$O)$_4$ (**7**).

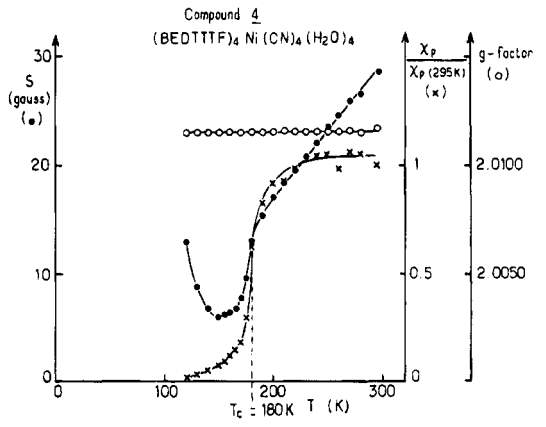

Figure 8. Temperature dependences of the *g* factor, ESR line width, and spin susceptibility for δ-(ET)$_4$[Ni(CN)$_4$](H$_2$O)$_4$ (**3**).

width and spin susceptibility T dependences. Apparently, two regime changes are occurring: a first one around 200 K which is detected only by the modification of the spin dynamic, i.e., a line-width narrowing, and a second one at 30 K which appears as a structural phase transition. Indeed in this temperature range, the spin susceptibility is decreasing sharply. This is characteristic of the opening of a gap at the Fermi level, i.e., of a low-dimensional structural instability giving rise to a diamagnetic and insulating ground state.

Concerning the α_2 phase, the experimental results are completely different in spite of strong structural analogies with the α_1 phase. Firstly the spin susceptibility *T* dependence obeys a classical Curie–Weiss law with a Weiss temperature $\theta = -25$ K, characteristic of rather weak antiferromagnetic interactions. This result is in agreement with the presence of strongly localized spins on a strongly dimerized stack which behaves as a regular magnetic chain with a weak intrachain exchange coupling constant as it is well known for some TCNQ salts.[19] Other experimental evidences are supporting this picture: on one hand, the poor dc conductivity observed for this compound (Figure 4b), and on the other hand the presence of a narrow ESR impurity line which appears after several temperature cycles. The supplementary line is due to defects induced by the thermal dilatation anisotropy and leading to an odd–even number of electrons in a given stack as described by the interrupted strand model.[19] In addition we observe a decrease of both components which can be associated with the presence of quasi-1D magnetic fluctuating regime but the interchain exchange coupling is also very weak and the condensation of a 3D magnetic ground state should occur at a very low Neel temperature only (T_N < 2 K).[20] Finally, the compound 4 representative of the δ phase has been examined (Figure 8). A rather sharp phase transition is observed through the line width and the spin susceptibility *T* dependences, in agreement with the dc conductivity experiments which reveal a conductor-insulator transition in the same temperature range (Figure 5).

Transfer Integrals, Band Structures, and Fermi Surfaces. The EH transfer integrals, band structures and Fermi surfaces are given in Table 5 and Figures 9–11 following the labeling defined on Table 2a,b for the transfer integrals.

α_1 phase: The transfer integrals are very similar for the Pt-based salt and the Pt/Ni alloy; see Table 5. The intrastack interactions (along the *c* direction) are small and show a larger dimerization for the A column than for the B–C column. The interstack interactions are slightly larger. The resulting band structures are thus almost identical for the two salts, and only results for the alloy system are shown in Figure 9. The band structure is indicative of a metallic character, and the Fermi level cuts the three upper bands. The small anisotropy of the transfer integrals leads to the large closed orbit located in the Fermi surface (FS) at the

(19) Hatfield, W. E.; Terhaal, W. *Annu. Rev. Mater. Sci.* **1982**, *12*, 177.

(20) Coulon, C. In *Organic and inorganic low dimensional crystaline materials*; Delhaes, P., Drillon, M., Eds.; NATO Assoc., **1987**, *168*, 201.

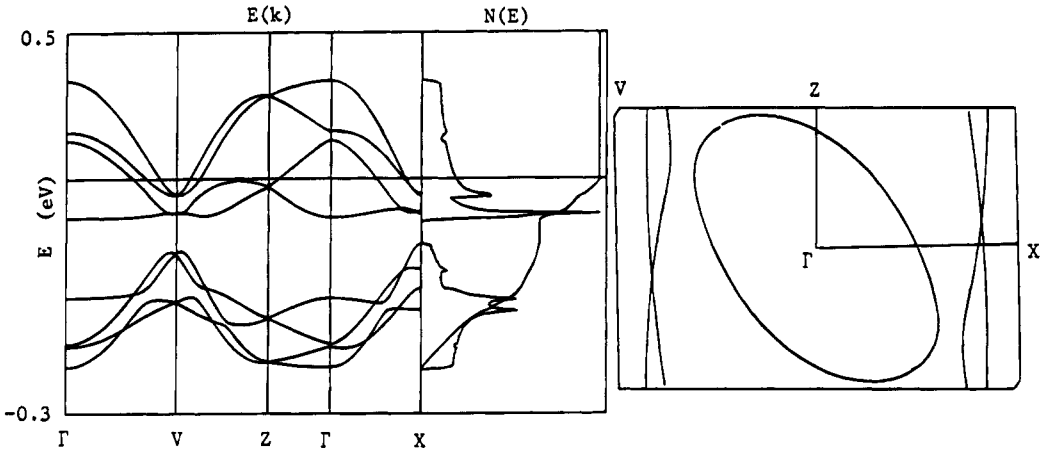

Figure 9. Dispersion energy $E(k)$, density of state $N(E)$, and Fermi surface for **5** calculated from the transfer integrals of Table 5.

Table 5. EH Transfer Integrals t (meV)[a] Calculated with the Double-ζ Basis Set[21]

compound	interaction	t (double-ζ)
1	c_1	20
	c_2	36
	p_4	94
	p_1	66
	p_3	60
	p_2	85
	c_3	18
	c_4	18
5	c_1	22
	c_2	35
	p_4	95
	p_1	55
	p_3	60
	p_2	87
	c_3	7
	c_4	7
3	b	−77
	a_1	193
	ab_1	−7
	ab_2	34
	a_2	145
4	b	−76
	a_1	190
	ab_1	−7
	ab_2	35
	a_2	158
6	b	−79
	a_1	192
	ab_1	−9
	ab_2	35
	a_2	146
7	a_1	0
	a_2	0
	b_1	79
	b_2	51
	b_3	74
	b_4	64

[a] In the case of **1**, **5** and **3**, **4**, **6**, the integrals labeling corresponds to that of Mori et al.[28] on α-$(ET)_2[MHg(SCN)_4]$.

center of the first Brillouin zone (BZ). The two other bands give rise to rather 1D lines close to the edge of the BZ. We have recently shown that the basis set quality (i.e., using single-ζ vs double-ζ Slater type orbitals as atomic orbitals)[21] may induce large changes in the band structure and Fermi surface of the α-$(ET)_2$-$[MHg(SCN)_4]$ (M = K, Rb, Tl, NH_4) series. This is due to the large variation of the transfer integral ratio c_1/c_2. This ratio also exhibits a strong sensitivity to the basis set in the present series. However, the band

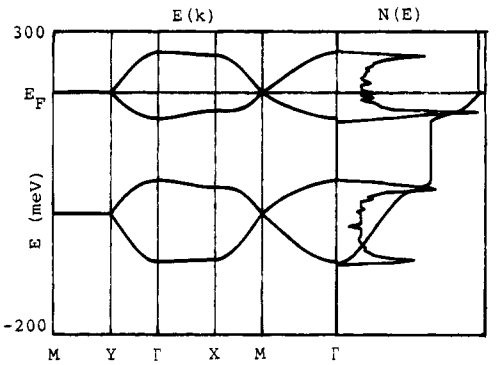

Figure 10. Dispersion energy $E(k)$, density of state $N(E)$ for **7** calculated from the transfer integrals of Table 5.

structure corresponding to double-ξ basis set (Figure 9) is qualitatively similar to the single-ξ basis set. By comparison of the Hg-based salts, in which different c_1/c_2 ratios generate different band structures and Fermi surfaces, this result might be related to the different space group of the crystals: the unit cell in the α_1 series contain eight ET molecules while there are only four molecules in the α-type Hg unit cell.

α_2 phase: The transfer integrals of the α_2-phase are roughly similar to the ones of the α_1-phase: they are quite small along the stack while the interstack integrals are found around 30 meV. The existence of independent molecules in the unit cell may result in some cases in different site energies which may be taken into account in the band structure as discussed previously.[22] For α_2, the calculated difference between the site energies of A and B amounts to 400 meV which is much larger than the transfer integrals. The corresponding value for the α_1 salts is only 160 meV between B and C. The associated band structure is given in Figure 10. There is an accidental degeneracy along the MY line, whose energy is the Fermi energy. As a consequence, the Fermi surface (not shown here) is made of two 1D parallel lines which nest perfectly.

δ-phase: In the case of the three structures, the molecules stack roughly in the c direction: see Figure 3a. But it is important to notice that the two intrastack packing modes of the ET molecules ($ab_1 = -7$ meV; $a_2 = 158$ meV), which are shown in Figure 3b, do not correspond to the largest integral, a_1. Besides, the

(21) Ducasse, L.; Fritsch, A. *Solid State Commun.* **1994**, *91*, 201.

(22) Ducasse, L.; Abderrabba, M.; Gallois, B.; Chasseau, D. *Synth. Met.* **1987**, *19*, 327.

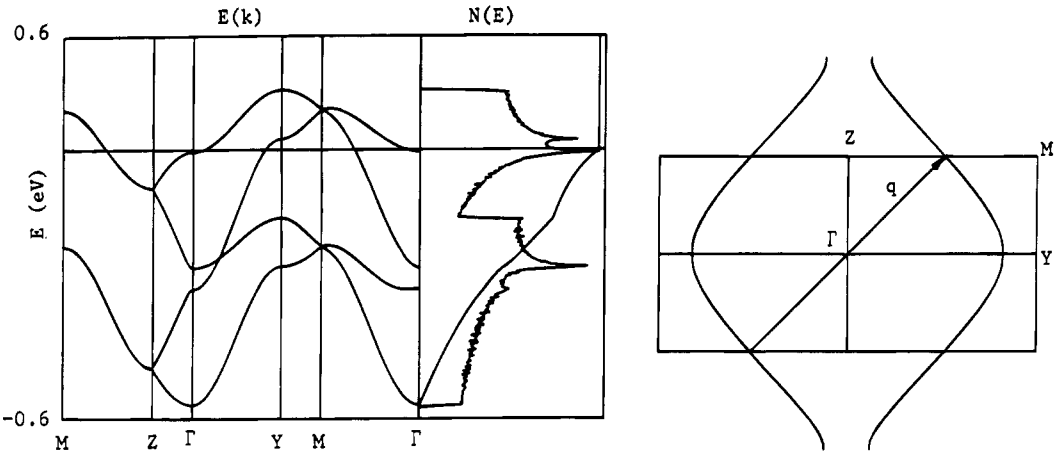

Figure 11. Dispersion energy $E(k)$, density of state $N(E)$, and Fermi surface for **6** calculated from the transfer integrals of Table 5. The Fermi surface is represented in the extended Brillouin zone.

integrals along b axis are negative and show smaller absolute values.

There are only slight differences between the transfer integrals in the series of the δ-phase. Consequently, the band structures and the Fermi surfaces are very similar for the whole series, so that only the results concerning the salt δ-(BEDT-TTF)$_4$[Ni(CN)$_4$]$_{0.48}$[Pt(CN)$_4$]$_{0.52}$(H$_2$O)$_4$ (**6**) are reported in Figure 11. There are four molecules per unit cell, neglecting interactions in the a direction, the dispersion energy may be obtained analytically due to symmetry considerations. The band width along the b^* direction is $4|t_b|$ ($t_b = -79$ meV for **6**), and it may be shown that the Fermi energy is given by the energy $E(b^*/4,c^*/2)$ which is 241, 247, and 241 meV for **3**, **4**, and **6**, respectively. The band structure and the Fermi surface are indicative of a pronounced 2D character shown by the warping of the Fermi surface, which is however open along the transverse direction.

Within the stack (along the c direction), two modes of packing are found: the first one involves two parallel ET molecules, while the second one involves a twisting angle of around 30°. These different modes of stacking invariably result in highly dimerized chains, as found in other ET salts: the α' phase (for example (ET)$_2$CuCl$_2$),[16b] (ET)$_2$MCl$_4$ (M = Fe or Ga),[23] and (ET)$_4$Cl$_2$,6H$_2$O.[24]

Discussion

Four different types of organic sublattices have been realized in the case of the ET/$[M(CN)_4]^{2-}$ system[2-3,25] (Figure 12) and so two main points concerning the molecular building of such system have been evidenced: Firstly the electrochemical crystal growth in aqueous mixtures yield as the major product the low conducting δ type but not the hydrated β phases reported to be superconducting under hydrostatic pressure and obtained in 1,1,2-trichloroethane/ethanol mixtures. The crystal growth mechanism of such interesting phase appears thus to be related to a critical water concentration. Second, the alloying made on the anionic

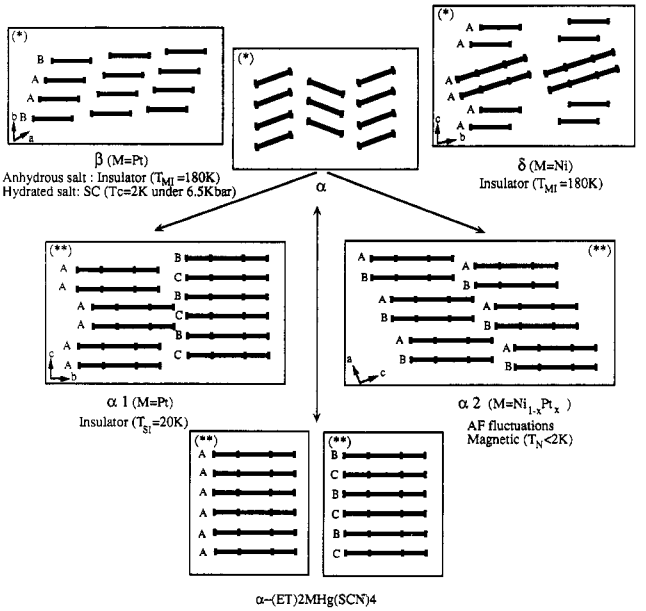

Figure 12. Schematic diagrams of the different structural types encountered in the ET/$[M(CN)_4]^{2-}$ system compared with α-(ET)$_2$[MHg(SCN)$_4$] and the different observed ground states. Views along the main (*) and minor (**) molecular axis of the ET unit are presented.

sublattice allowed the stabilization of a molecular structural type (α_2) apparently not achievable with the pure anionic precursors. Therefore the alloying volume effect seems to offer a highest degree of liberty to the cationic units in building new structural packings which could afford interesting materials.

α-phases: Three kinds of packing are observed for the α phase, namely, the α, α_1, and α_2 (see Figure 12). The band structure agrees qualitatively with the weak metallic character observed at room temperature. The low-temperature semiconducting regime contrasts with the corresponding data in other α-phases, and in particular in α-(ET)$_2$[MHg(SCN)$_4$], which remains metallic down to very low temperature, at which a superconducting ground state (M = NH_4^+) or an antiferromagnetic ground state (M = alkaline atom) may be observed.[26,27] Two qualitative differences distinguish the two series:

(23) Mallah, T.; Hollis, C.; Bott, S.; Kurmoo, M.; Day, P.; Allan, M.; Friend, R. H. *J. Chem. Soc., Dalton Trans.* **1990**, 859.
(24) Rosseinsky, M. J.; Kurmoo, M.; Day, P.; Marsben, I. R.; Friend, R. H.; Chasseau, J.; Gaultier, J.; Bravic, G.; Ducasse, L. *J. Mater. Chem.* **1993**, *3*, 807.
(25) Fettouhi, M.; Ouahab, L.; Grandjean, D.; Toupet, L. *Acta Crystallogr.* **1992**, *B48*, 275.
(26) Wang, H. H.; Carlson, K. D.; Geiser, U.; Kwok, W. K.; Vashon, M. D.; Tompson, J. E.; Larsen, N. F.; McCabe, G. D.; Hulsher, R. S.; Williams, J. M. *Physica C* **1990**, *166*, 57.

(i) The interstack dihedral angles are significantly lower than the corresponding values observed in metallic systems which exhibit the superconducting α and θ-$(ET)_2X$ salts[1] and also the metallic α phases such as $ET_2[MHg(SCN)_4]$ (M = alkaline atom)[28] or the phase I of $ET_2Ag(CN)_2$[29] (around 80°) but they are roughly similar to the values (less than 50°) found in the phase II of $ET_2Ag(CN)_2$[29] which undergoes a metal–insulator transition and also in the newly synthesized α_1 and α_2 semiconductor salts of ET with polyoxometalate anions.[13]

(ii) The crystal symmetry is the same for both series, but the content of the 2D unit cell in the ET layer (*ac* plane) is twice as large in the case of α_1-$(ET)_4[Pt(CN)_4]_{1-x}[Ni(CN)_4]_x$ (eight ET molecules) as in $(ET)_2[MHg(SCN)_4]$ (four ET molecules). The origin of this difference lies on the fact that, in the salts under study, the packing of the A column is built from dimeric units (c_1 interaction) and the overlap (c_2) between these units is different from the intradimer overlap; see Figure 1. It is important to note that this structural feature is also present in the α_1 and α_2 salts of ET with polyoxometalate anions.[13] This last point might be quite important with regard to the electronic description. The smooth change from a metallic conductivity to a semiconducting regime is reminiscent of more 1D organic salts, like the $(TMTTF)_2X$ series.[30] In the latter case, no change in the crystal symmetry may be observed for the temperature range at which the localization takes place. Consequently, a mechanism based on the nesting of the Fermi surface may not be invoked. Besides, the effects of the electron–electron correlation are certainly important in organic systems. The analysis of such effects in 1D 3/4-filled bands has been performed recently within an extended Hubbard hamiltonian.[31] For salts exhibiting a dimerized structure, the weaker bond is weakened by the correlation while the stronger one is only slightly modified, so that the localized regime corresponds to a strong bond order wave (BOW) mechanism. In the present case, the dimerization ratio is related to the c_1/c_2 ratio which has been shown to depend on details of the crystal structure[21] (this ratio is 1.5 using a double-ξ basis set (Table 5) but increases to 28 with a single-ξ basis set!)

The unit cell of the α_2-phase contains four ET molecules as in the case of the α metallic salts. However there is only one type of dimerized chain. Contrary to the previous case, the localization in the α_2 phase is certainly related to the existence of stacks containing A and B molecules with different charges which induce a charge density wave (CDW). Moreover the existence of dimerized chains may be related to the room-temperature electrical conductivity which decreases with the number of such chains in the unit cell: two regular chains for α, one regular, and one dimerized for α_1 and two dimerized for α_2.

δ-Phase: The band structure results obtained from the 300 K crystal data agree with the observed high temperature metallic behavior. The Fermi surface of Figure 11 exhibits rather straight lines which may be well nested by the nesting vector **q**. The existence of this nesting might be related to the occurrence of the phase transition observed in the δ phase (see Figure 8). As previously mentioned, the transfer integrals, band structures, and Fermi surfaces of the δ-series are very close to the corresponding data obtained for $(ET)_4Cl_2,6H_2O$,[24] which also exhibits a metal-to-semiconducting transition and for which the resistivity minimum is not accompanied by any structural transition. This may be contradictory with the EH one-electron model, which involves a Peierls-type transition driven by the gap opening at the Fermi level through the FS nesting. As in the case of the α_1 phase the localization may be ascribed to a BOW mechanism. In the δ-series, the ratio between the intra- and interdimer integrals is around 1.3 (see Table 5), while it is 1.5 in $(ET)_4Cl_2,6H_2O$. These dimerization ratios are close to the values found in $(TMTTF)_2X$ series, which show similar evolution of the conductivity with temperature.[30] A comparison should also be done with the β phase which undergoes a metal insulator transition below 250 K[2,3] and trying to explain the origin of such transition Rovira et al. and Martin et al.[32,33] suggest, in the absence of a low-temperature structural transition, an electronic localization mechanism as in the α phase compounds.

The similarities between the band structures of δ-$(ET)_4[Ni(CN)_4]_{1-x}[Pt(CN)_4]_x(H_2O)_y$ on one hand, and $(ET)_4Cl_2{\cdot}6H_2O$, on another hand, are independent of the crystal symmetry, which is monoclinic (*P2/c*) in the first case, and orthorhombic (*Pcca*) in the second case. However, the physical properties show contrasted behaviors. First, the room-temperature conductivities differ by more than 2 orders of magnitude. The temperature dependences of the conductivity are also different: for the Cl salt, it is almost constant down to around 160 K and then shows a small temperature-dependent activation energy, while the localization takes place already around 200 K for the δ-phase. Second, the magnetic measurements are also different. In the case of Cl, the spin and static susceptibilities are temperature independent between 300 and 70 K and obey a Curie–Weiss law below 50 K with Θ = −4 K. For the δ phase, there is a transition at 180 K which is clearly seen in the ESR measurements (see Figure 8).

Concluding Remarks

We have prepared several radical cation salts of BEDT-TTF with square-planar diamagnetic organometallic dianions based on Ni and Pt. Electrocrystallization in different experimental conditions enables us to isolate and characterize new phases of the α_1, α_2, and δ type but not yet a κ-type phase. We have also shown that this rich polymorphism which presents always the same degree of ionicity (ϱ = 0.5) is independent of the anion transition metal (pure or alloyed); for example, rather similar results have been found by Kurmoo et

(27) Oshima, M.; Mori, H.; Saito, G.; Oshima, K. *The Physics and Chemistry of organic superconductors*; Saito, G., Kagoshima, S., Eds.; Springer-Verlag: Berlin, 1990; p 257.
(28) (a) Oshima, M.; Mori, H.; Saito, G.; Oshima, K. *Chem. Lett.* **1989**, 1159. (b) Mori, H.; Tanaka, S.; Oshima, M.; Saito, G.; Mori, T.; Maruyama, Y.; Inokushi, H. *Bull. Chem. Soc. Jpn.* **1990**, *63*, 2183.
(29) Kurmoo, M.; Talham, D. R.; Pritchard, K. L.; Day, P.; Stringer, A. M.; Howard, J. A. K. *Synth. Met.* **1988**, *27*, A177.
(30) Delhaes, P.; Coulon, C.; Amiell, J.; Flandrois, S.; Toreilles, E.; Fabre, J. M. *Mol. Cryst. Liq. Cryst.* **1979**, *50*, 43.
(31) Fritsch, A.; Ducasse, L. *J. Phys. I* **1991**, *1*, 855.
(32) Rovira, C.; Whangbo, M. H. *Synth. Met.* **1993**, *60*, 145.
(33) Martin, J. D.; Doublet, M. L.; Canadell, E. *J. Phys.* **1993**, *3*, 2451.
(34) Kobayashi, H.; Kobayashi, A.; Sasaki, Y.; Saito, G.; Inokushi, H. *Bull. Chem. Soc. Jpn.* **1986**, *59*, 301.
(35) Triki, S.; Ouahab, L.; Grandjean, D.; Fabre, J. M. *Acta Crystallogr.* **1991**, *C47*, 645.

al. using silver cyanide counterion.[36] The factors which determine the donor packing arrangement are very subtle because we can see at first glance that the unit cell volume per unit of BEDT-TTF is constant within this series as already noticed for the outstanding series of triiodide salts (α, β, θ, and κ phases[1]). Following Mori et al. approach,[37] we can see that an effective volume associated to the ET donor molecules can be calculated after subtracting the anionic volume from the unit cell one. It inverse value furnishes the electronic charge concentration which is clearly a basic quantity for a conducting or even a low temperature SC state. However we see that for these metallocyanate salts (Pt, Ni, Pd, and Ag)[3,36] with almost the same electron concentration as for the iodide salts,[38] we observe different types of low-T states. It appears therefore that the physical properties of these phases have to be associated with the details of the electrostatic and electronic interactions. The cohesive energy is due to a delicate balance between the rather 3d Madelung energy and the essentially 2d and 1d covalent bonding as described by the EHT band structures which takes account only of the topology of the electronic interactions. We have described a larger variety of Fermi surfaces going from quasi-1d open surface characterized by the presence of nesting vector (δ phase) to almost 2d system with a closed FS (α_1 phase). However, it is not possible to ascribe all the observed low-temperature ground states to these effects alone. It is also necessary to take account of the specific anion–cation interactions. A remarkable demonstration of such an effect is given by the salts of the β-series with the $[Pt(CN)_4]^{2-}$ or $[Ni(CN)_4]^{2-}$ dianions. It has been observed that a metallic state is present down to a very low temperature for the Pt (or Ni) hydrated salts undergoing a superconducting phase transition at 2K under hydrostatic pressure.[6] This behavior differs strongly from the semiconducting states observed in the anhydrous series. If we compare the room temperature unit cell volumes and the corresponding effective volumes for the anhydrous and hydrated salts, we calculate an increase of about 7% (ΔV = 90 Å^3) with the introduction of one water molecule. This value is several times larger than expected (water molecule volume is about 15 Å^3) and is not observed in some other series.[36] It thus might be in relation with the observed changes from a metallic regime to a localized one in the isomorphous salts. The introduction of water molecules in the structure would change the electrostatic term (for instance via hydrogen bonding with the terminal CH_2 groups of ET molecules) which would be balanced by a modification of the covalent energy associated with the overlap of the π orbitals. It is also possible that the molecular site energies of the two independent molecules would be more or less differentiated due to a different neighbouring of water molecules.

To conclude the large variety of electronic states occurring in these salts (see Figure 12) might originate from the constraints opposed to the 2d electronic gas by the electrostatic field issued from the anion–cation interactions. This situation could be reminiscent of a Wigner crystallization in atomic solids.[39] Thus several metastable phases, corresponding to very similar electron densities and effective volumes, are possible, giving rise to a chameleon structural chemistry in these molecular solids.

Supplementary Material Available: Crystallographic data (26 pages); observed and calculated structure factors (91 pages). Ordering information is given on any current masthead page.

CM940268N

(36) Kurmoo, M.; Pritchard, K. L.; Talham, D. L.; Day, P.; Stringer, A. M.; Howard, J. A. K. *Acta Crystallogr.* **1990**, *B46*, 348.

(37) Mori, H.; Tanaka, S.; Oshima, M.; Saito, G.; Mori, T.; Maruyama, Y.; Inokuchi, H. *Bull. Chem. Soc. Jpn.* **1990**, *63*, 2183.

(38) In all these ET salts with ϱ = 0.5, the effective volume, i.e., the formal volume occupied by a mixed valence dimer $(D)_2^{\bullet+}$ is around (700 ± 15) Å^3. This value corresponds to a rather low electronic concentration of 1.3 × 10^{21} cm^{-3}.

(39) Mott, N. F. *Metal-Insulator transitions*, 2nd ed.; Taylor and Francis: 1990.